Repeatable high-resolution statistical downscaling through deep learning

Dánnell Quesada-Chacón[1], Klemens Barfus[1], and Christian Bernhofer[1]

[1]Institute of Hydrology and Meteorology Technische Universität Dresden, Germany

Correspondence: Dánnell Quesada-Chacón (dannell.quesada@tu-dresden.de)

Abstract. One of the major obstacles for designing solutions against the imminent climate crisis is the scarcity of high spatio-temporal resolution model projections for variables such as precipitation. This kind of information is crucial for impact studies in fields like hydrology, agronomy, ecology and risk management. The currently highest spatial resolution datasets on a daily scale for projected conditions fail to represent complex local variability. We used deep learning based statistical downscaling methods to obtain daily 1 km resolution gridded data for precipitation in the Eastern Ore Mountains in Saxony, Germany. We built upon the well established `climate4R` framework, while adding modifications to its base-code and introducing skip connections based deep learning architectures, such as *U-Net* and *U-Net++*. We also aimed to address the known general reproducibility issues by creating a *containerized* environment with multi-GPU and `TensorFlow`'s *deterministic* operations support. The perfect prognosis approach was applied using the *ERA5* reanalysis and the *ReKIS* (Regional Climate Information System for Saxony, Saxony-Anhalt, and Thuringia) dataset. The results were validated with the robust VALUE framework. The introduced architectures show a clear performance improvement when compared to previous statistical downscaling benchmarks. The best performing architecture had a small increase in total number of parameters, in contrast with the benchmark, and a training time of less than 6 minutes with one NVIDIA A-100 GPU. Characteristics of the deep learning models configurations that promote their suitability for this specific task were identified, tested and argued. Full model repeatability was achieved employing the same physical GPU, which is key to build trust in deep learning applications. The EURO-CORDEX dataset is meant to be coupled with the trained models to generate a high-resolution ensemble, which can serve as input to multi-purpose impact models.

Keywords: climate change, statistical downscaling, perfect prognosis, ERA5, Ore Mountains, deep learning, repeatability, GPU determinism

1 Introduction

The Earth has undoubtedly warmed at an alarming rate in recent decades (IPCC, 2021), with the last one, 2011-2020, being the warmest on record. The last seven years (2015-2021) have been the warmest on record as well, while 2020, tied with 2016, was the hottest (WMO, 2022). Notably, during 2020 the Pacific Ocean entered a La Niña phase, which conveys an overall cooling effect, in contrast to the El Niño warming conditions observed in 2016 (Voosen, 2021), which can be seen as a strengthening of the warming trend by man-induced climate change. The above mentioned facts are based on global averages. On a smaller

scale, there have been several signs of the effects that climate change can have on extreme events, e.g. the 2020 fires in Siberia, California and Australia; the 2021 summer flash floods events in Western Europe and China; and the 2021 summer heat waves on the northern hemisphere soon after observing the coldest April in Germany for decades.

Climate change is one of the greatest challenges faced by mankind and General Circulation Models (GCMs) are the best tools available to model the response of the climate system to different forcing scenarios. Nevertheless, despite the remarkable improvements of GCMs over recent years, their spatial resolution yields their output unfit to be used directly for regional climate change impact studies in fields such as hydrology, agronomy, ecology and risk management (Maraun and Widmann, 2018). The resolution of GCMs can be of up to a few hundred kilometers, depending on the GCM generation, which results in large regional biases when contrasted to station data (Flato et al., 2013). To overcome this hindrance, downscaling methodologies are employed, which transform coarse GCM output to regional and local scale (von Storch et al., 1993).

Dynamical downscaling uses the initial and boundary conditions from GCM output to drive high-resolution Regional Climate Models (RCMs) (Hallett, 2002). The Coordinated Regional Climate Downscaling Experiment (CORDEX, 2021) offers multiple RCM output variables at daily temporal resolution based on CMIP5 (Taylor et al., 2012) projections with a spatial resolution of 0.44, 0.22 and 0.11° (approximately 50, 25 and 12.5 km, correspondingly), with the highest resolution being available only for Europe. Regardless these great efforts and the improved performance on the regional level of the 0.11° against the 0.44° models (Pastén-Zapata et al., 2020), the resolution still does not meet the needs of impact modellers, which can be a few kilometers or less, particularly for topographically complex regions.

Statistical downscaling methods build empirical relationships or *transfer functions* between the larger-scale atmospheric variables (predictors) and regional or local-scale variables (predictands) (Hewitson and Crane, 1996; Maraun and Widmann, 2018), such as precipitation or temperature. Perfect prognosis is the particular statistical downscaling methodology used in the present study, which requires a daily correspondence between predictors and predictands. Statistical downscaling implementations have significantly evolved since the 1990s through technological advances, with increasing amounts of input data, performance, complexity, and computational demands. Consequently, several methods have been studied for statistical downscaling, e.g. linear models for station data (paired with canonical correlation analysis, von Storch et al., 1993); artificial neural networks (ANNs, Hewitson and Crane, 1996; Wilby and Wigley, 1997; Cavazos and Hewitson, 2005); support vector machines (Tripathi et al., 2006; Pour et al., 2016); random forest (He et al., 2016; Pang et al., 2017); and, recently, modern ANNs architectures and deep learning techniques for gridded data (Vandal et al., 2018; Baño-Medina et al., 2020; Höhlein et al., 2020; Serifi et al., 2021).

Baño-Medina et al. (2020) provided a comparison between several deep learning models and more classical methods, such as generalized linear models, while validating the results with a robust framework such as VALUE (Maraun et al., 2014; Gutiérrez et al., 2019). Baño-Medina et al. (2020) also introduced the `downscaleR.keras` *R* package, which enables the use of the `Keras` (Chollet et al., 2015) and `TensorFlow` (Abadi et al., 2015) machine learning libraries in `climate4R` (Iturbide et al., 2019). Even though deep learning methods were examined in the aforementioned paper, the applied models do not exploit modern convolutional neural networks (CNNs) architectures, like skip or residual connection based models (Srivastava et al., 2015) such as *U-Net* (Ronneberger et al., 2015) and *U-Net++* (Zhou et al., 2018), which allow state-of-the-art performance in

computer vision assignments. Additionally, since the study was developed for whole Europe with intercomparison purposes, the target resolution of the statistical downscaling method is too coarse (0.5°) for impact studies.

Furthermore, *reproducibility* is at the core of good scientific practices, yet, it is a challenging feature to achieve in several scientific areas. Stoddart (2016) states that from a poll of 1500 scientists more than 70% of researchers were not able to reproduce another scientist's experiment and more than half were unsuccessful reproducing their own experiments. Especially *reproducibility* is a known issue for climate modelling (Bush et al., 2020) and also for calculations carried out on GPU systems (Jézéquel et al., 2015; Nagarajan et al., 2018; Alahmari et al., 2020), particularly when applying machine learning frameworks that do not guarantee *determinism*.

Reproducibility is a term that is not standardized in the scientific literature. Depending on the source, field and circumstances, *repeatability* and *replicability* are employed (Rougier et al., 2017; Nagarajan et al., 2018; Association for Computing Machinery (ACM), 2021), which undoubtedly leads to confusion. The ACM adopted the three terms based upon the definition in the International Vocabulary of Metrology (Joint Committee for Guides in Metrology, 2006) for conditions of a measurement. Under the ACM terminology, repeatability implies the same measurement precision by the same team and the same experimental set-up. This is the only condition achievable within any singular publication, since the other two involve another independent team. Despite their conflicting definitions respectively focused on computer science and deterministic deep learning, both Rougier et al. (2017) and Nagarajan et al. (2018) allowed discrepancies between observations if the results are *qualitatively* the same or *equivalent*, which can be particularly relevant for deep learning applications. Additionally, Goodman et al. (2016) proposed *methods reproducibility*, *results reproducibility*, and *inferential reproducibility* to address this nomenclature confusion. Analogously, only *methods reproducibility* is achievable within any publication and this implies to provide "enough detail about study procedures and data so the same procedures could, in theory or in actuality, be exactly repeated" (Goodman et al., 2016).

Due to its less conflictive definition and what is achievable within a publication, repeatability will be pursued hereafter. Still, *general reproducibility* will be employed for broader use of the terminology. The concept of "qualitatively the same" or "equivalent" results will be referred to as *similarity*, to avoid consensus with conflicting definitions. Also, we aspire to comply with the methods reproducibility condition of Goodman et al. (2016). For a more comprehensive overview on the general reproducibility related terminology, the reader is referred to Plesser (2018).

`TensorFlow` is the deep learning framework employed in the `downscaleR.keras` *R* package and in `climate4R`. To our knowledge, there is limited scientific literature on the repeatability capacities of `TensorFlow` on GPU systems. Nagarajan et al. (2018) dealt with the sources of non-determinism for both `PyTorch` and `TensorFlow` deep learning frameworks, but could not achieve determinism with the latter and, therefore, neither repeatability. Alahmari et al. (2020) were able to use the deterministic implementations of some `TensorFlow` algorithms with versions 1.14 and 2.1, yet, could only achieve repeatability with v2.1 using the *LeNet-5* model but not with an *U-Net*. Nevertheless, newer versions of `TensorFlow` have included further deterministic implementations of GPU algorithms (NVIDIA, 2021).

The aim of this paper is to apply the statistical downscaling methodology for precipitation in the Eastern Ore Mountains employing as predictors the *ERA5* reanalysis (Hersbach et al., 2020) and as predictands the *ReKIS* (Regional Climate Infor-

mation System for Saxony, Saxony-Anhalt, and Thuringia) dataset, generated at the Chair of Meteorology of the Technische Universität Dresden (Kronenberg and Bernhofer, 2015) in order to develop and validate transfer functions under modern deep learning architectures. These transfer functions can be subsequently used to downscale a climate projection ensemble directly from dynamically downscaled data (e.g. CORDEX model output), rather than from GCMs, as in Quesada-Chacón et al. (2020),

100 to a suitable scale for multi-purpose climate change impact models. The rationale of building on top of the `climate4R` framework in a *containerized environment* is to ease and verify its repeatability, an imperative which we intend to deepen, shed light upon and standardise for further research.

This paper is structured as follows: section 2 presents details of the datasets employed as predictors and predictands. In section 3, we describe the downscaling methodology, the models used to create the transfer functions , the tools employed to

105 evaluate the models, the hardware and software used, and the experimental workflow to assess the repeatability. The section 4 presents the results and discussion related to the performance of the models and to the general reproducibility of the results. Lastly, section 5 renders a summary of the investigation, its conclusions and further research outlook.

2 Data

2.1 Focus region

110 The Ore Mountains, as the study area of the present paper, is a transnational mountain range that acts as a natural border between Germany and the Czech Republic. It is a region with rich mining history and multiple resources. On the German side, the range is part of the Ore Mountains/Vogtland Nature Park, established in 1990 with an area of 1495 km^2, of which 9% corresponds to settlements, 30% to agriculture and 61% to forests. The highest points on the German side are the Fichtelberg (elevation 1215 m) and the Kahleberg (elevation 905 m) in the Eastern Ore Mountains. The Ore Mountains contain five

115 biotopes that provide invaluable ecosystem services to the region. Particularly, the Eastern Ore Mountains are characterized by the species-rich mountain meadows biotope, which offers recreation, wildlife observation chances, distinctive scenery and herbs for medical purposes (Bastian et al., 2017). The Eastern Ore Mountains are the present focus region (see Figure 1a).

2.2 Predictands

A subset of the ReKIS (2021) gridded dataset for the Free State of Saxony was used as predictand, which has a spatial

120 resolution of 1 km at a daily temporal resolution. This dataset uses station data from the German Meteorological Service (Deutscher Wetterdienst, DWD) and the Czech Hydrometeorological Institute (CHMI) as source (Kronenberg and Bernhofer, 2015). There are several variables available from this dataset, nevertheless the present project focuses on precipitation.

The raw station data for precipitation was corrected after Richter (1995) and interpolated using Indicator Kriging (Deutsch and Journel, 1998) for the probabilities of precipitation. Ordinary Kriging (Wackernagel, 2010) with a negative weight correc-

125 tion and exponential semivariogram model according to Deutsch (1996) was employed to estimate the amounts of precipitation.
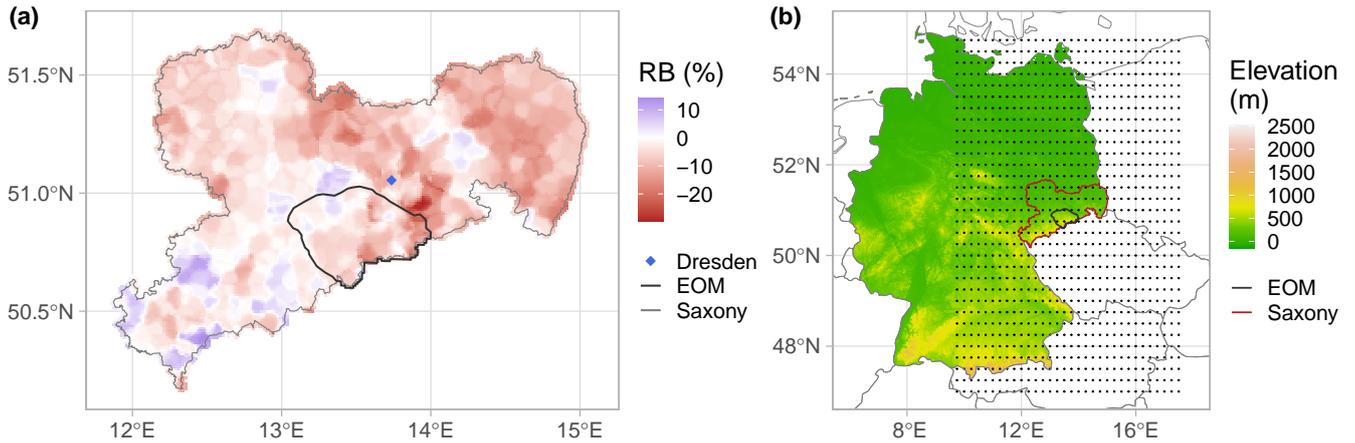
Figure 1. Location of the study region and the predictor's domain. **(a)** Relative bias (RB) of precipitation between training and validation periods for the whole *ReKIS* domain for Saxony. The study region, Eastern Ore Mountains, abbreviated as EOM in the figure, is inside the darker gray line. **(b)** Topography of Germany, the center of the ERA5 sub-domain pixels (marked by dots, 32 by 32) used for the predictors and the Eastern Ore Mountains.

The gridded dataset ranges from 1960 until 2015. The original *ReKIS* dataset for Saxony (shown in Figure 1a) was cropped to the Eastern Ore Mountains region, giving a region with 1916 pixels to be modelled.

2.3 Predictors

The reanalysis dataset employed as predictors is ERA5 (Hersbach et al., 2020), which has a spatial resolution of 0.25°, 137
model levels interpolated to pressure levels and hourly temporal resolution. In this study the dataset from 1979 onwards was
employed to train the transfer functions . The atmospheric variables used, as in Baño-Medina et al. (2020), are zonal and
meridional wind, temperature, geopotential, and specific humidity at the 1000, 850, 700 and 500 hPa levels, for a grand total
of 20 different variables. The ERA5 dataset was aggregated to daily resolution and was further cropped to a 32 by 32 pixels (8
by 8°) domain size, centered over the Eastern Ore Mountains as displayed in Figure 1b.

3 Methods

3.1 Statistical Downscaling

As previously mentioned, we built on top of the `climate4R` framework, particularly on the code made available by Baño-
Medina et al. (2020), since it provides a great number of tools and the robust validation framework VALUE (Maraun et al.,
2014; Gutiérrez et al., 2019). The code needed to recalculate the results to be presented can be found on *Zenodo* (Quesada-
Chacón, 2022a), with all the modifications and extensions derived for our approach.

Statistical downscaling methods create a relationship between the predictors **x** and the predictands **y** by a statistical model *F(.)* or transfer function (Maraun and Widmann, 2018). Under the perfect prognosis approach, the calibration of the transfer functions is performed with "perfect" reanalysis predictors $\mathbf{x}_{ERA5}$ characterized by temporal correspondence with the observed data $\mathbf{y}_{ReKIS}$. The variables chosen (see subsection 2.3) have shown a high predictive power for Europe (Baño-Medina et al., 2020).

The period from 1979 to 2009 was used to train the transfer functions and the one between 2010 and 2015 as hold-out validation dataset. The reason for this training-validation split lies in the interest of evaluating the performance of the transfer functions under extrapolation conditions, since there has been a change in the precipitation regime between both time periods. This change tends to on average drier conditions in the training period, as observed in Figure 1a, where the relative bias is calculated as $(\overline{Pr_{Train}} - \overline{Pr_{Val}})/\overline{Pr_{Train}}$ with $\overline{Pr_{Train}}$ and $\overline{Pr_{Val}}$ the averaged daily precipitation of training and validation period, respectively. Notably, the latter might be significantly influenced by the 2013 summer floods, where the Eastern Ore Mountains was a focal point of heavy precipitation within Saxony. Also, the dataset does not include observations from 2015 until today, including the period from 2018-2019 where a long lasting drought was observed (Mühr et al., 2018).

3.2 Transfer functions

Baño-Medina et al. (2020) demonstrated that deep learning architectures improved the performance of the transfer functions when compared to "classic" models (linear and generalized linear models), attributable to the capacity of the CNNs to learn from the spatial distribution and patterns of the input layers. Particularly, the *CNN1* architecture was the best overall for precipitation. Its topology consist of three layers of CNNs, with 50, 25 and 1 filters or feature channels, respectively, which in terms of state-of-the-art deep learning is a rather simple architecture. Therefore, there is room for improvement for the transfer functions under more recent architectures, such as *U-Net* (Ronneberger et al., 2015), which was developed for biomedical image segmentation implementing skip connections, and *U-Net++* (Zhou et al., 2018). The latter is an iteration of the *U-Net* with improved skip connections between layers, translating usually to a better performance (Harder et al., 2020). Both architectures introduce a contraction path, also known as encoder, and a symmetric expansion path, the decoder (see Figure 2).

The encoder path reduces the spatial data contained in the input layers while increasing the feature information. The expansion path decodes the features obtained from the previous steps to match the target domain size. The skip connections provide access to the intermediate information contained in the features of the previous layers while smoothing the loss landscape (Li et al., 2018), which in turn, speeds up the training process.

The depth of the skip connections based architectures was a variable to optimize. Therefore, both architectures were tested under a three, four and five layers arrangement. Several numbers of starting feature channels were tested. The basic "convolutional unit" (*ConvUnit*) consisted of a convolutional layer (kernel size 3 by 3), with the respective activation function and, optional batch normalization and spatial drop-out. The last two options are used to avoid overfitting of the model. Batch normalization standardizes the layer's input data, which also improves learning speed, while spatial drop-out (2D version of `Keras`) randomly ignores entire feature maps during training. Two successive *ConvUnits* constitute a "convolutional block" hereafter referred to as *ConvBlock*.

(a) U-Net

(b) U-Net++
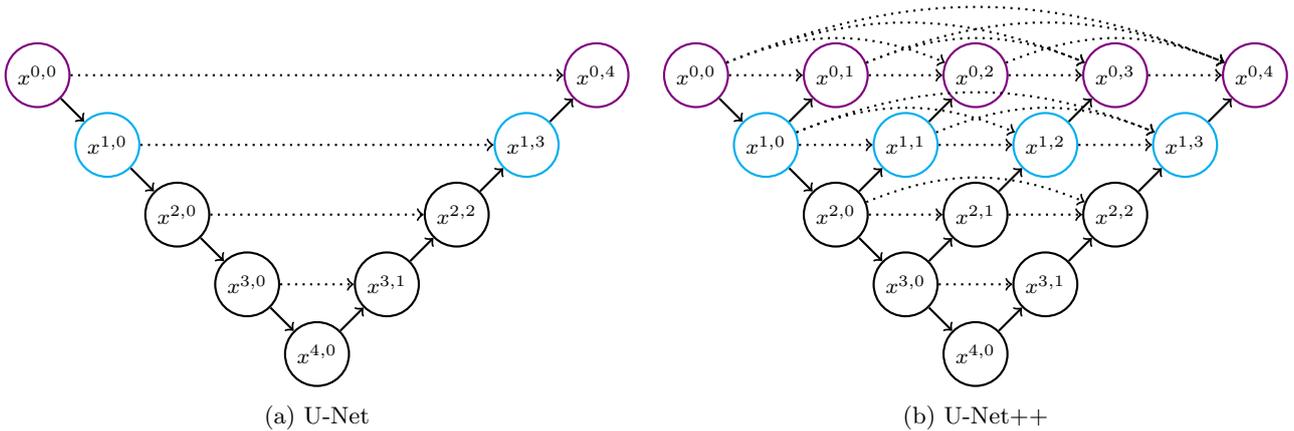
Figure 2. Skip connection based models tested for the transfer functions . The three layer version of each model is made up of only the black coloured nodes, the four layer version of the black plus the cyan nodes, and the five layer version of all of them. The $\searrow$ represents *down-sampling*, the $\nearrow$ *up-sampling* and the $\dashrightarrow$ *skip connections*. The nodes $x^{i,j}$ represent the *ConvBlocks*.

175   On the contraction paths, for each node a *ConvBlock* was applied, followed by a max pooling layer (2 by 2 pool size) or *down-sampling*. All the previous layers used the `padding = "same"` setting of `Keras`. On the decoder path, a transposed convolutional layer was employed, halving the number of channels of the previous layer with a kernel size of 2 by 2 (*up-sampling*). Subsequently, all the respective skip connections for each node are concatenated and then another *ConvBlock* is applied to the resulting concatenation.

180   After processing all the respective nodes and layers, a single *ConvUnit* with a 1 by 1 kernel size and no spatial dropout is applied. Several combinations of activation functions and feature channels were tested for this last *ConvUnit*. Then, as in Baño-Medina et al. (2020), the target function to optimize is the *Bernoulli Gamma* probability distribution function $f(y; \rho, \alpha, \beta)$ (Cannon, 2008, see Equation 1), and here especially the negative log-likelihood of it (Equation 2). The probability of rain occurrence ρ and the distribution parameters α (shape) and β (scale) were computed for each pixel. All of the tested

185   combinations of skip connection-based models were then compared to the best performing architecture from Baño-Medina et al. (2020), *CNN1*. Also other models similar to *CNN1* were added for examination i.e., *CNN32-1* consisting of three CNNs layers of 32, 16 and 1 filters; *CNN64-1* comprising four CNNs with 64, 32, 16 and 1 channels; and lastly, *CNN64_3-1* with 64, 32 and 1 features.

$$
f(y; \rho, \alpha, \beta) = \begin{cases} 1 - \rho & \text{if} \quad y = 0 \\[2ex] \dfrac{\rho \cdot (y/\beta)^{\alpha-1} \cdot e^{-y/\beta}}{\beta \cdot \Gamma(\alpha)} & \text{if} \quad y > 0 \end{cases} \tag{1}
$$

$$
-lnf = \begin{cases} -\ln(1 - \rho) & \text{if} \quad y = 0 \\[2ex] \dfrac{\alpha \cdot \ln\beta + \ln\Gamma(\alpha) + y/\beta}{\ln\rho + (\alpha - 1) \cdot \ln y} & \text{if} \quad y > 0 \end{cases} \tag{2}
$$

Several activation functions were tested e.g. *Sigmoid*, *ReLu* (Xu et al., 2015), *Leaky ReLu* (α = 0.3, see Equation 3) and a linear function. Spatial drop-out ratios of 0, 0.25 and 0.5 were also examined. The optimizer used is *Adam* (Kingma and Ba, 2015), for which different learning rates were explored. The *patience* for the early stopping criteria was also a variable. In addition several batch sizes were employed according to the available memory of the graphic processing units (GPUs). Throughout the calibration process of the models 90% of the data was randomly selected for training and the remaining 10% was used for during-training validation.

$$
\text{Leaky ReLu}(x) = \begin{cases} x & \text{if} \quad x > 0 \\[2ex] \alpha \cdot x & \text{otherwise} \end{cases} \tag{3}
$$

3.3 Model evaluation

In order to work under comparable conditions, the metrics employed in the present study correspond to the ones used by Baño-Medina et al. (2020) included in the VALUE framework (Maraun et al., 2014; Gutiérrez et al., 2019), which allows to validate numerous aspects such as extremes and the spatio-temporal structure. Among these metrics are: the relative bias, for both the mean and the 98th percentile, calculated both under deterministic and stochastic approaches; the root mean square error (RMSE); the temporal Spearman correlation; the ROC skill score (Manzanas et al., 2014); the bias of the median wet (WetAMS) and dry (DryAMS) annual max spells; as well as the bias of the relative amplitude of the annual cycle, using a 30 days moving window. A summary of the metrics is shown in Table 1, alongside with their units.

3.4 Hardware

The models were trained on the *Alpha Centauri* sub-cluster of the Center for Information Services and High Performance Computing (ZIH) of the Technische Universität Dresden, which consists of 34 nodes, each one with 8 NVIDIA A-100 (40 GB), 2 AMD EPYC 7352 (24 cores), 1 TB RAM and 3.5 TB of local NVMe memory. This single sub-cluster ranks as 242nd on the TOP500 (2022) supercomputer list of June.

Table 1. Metrics selected from VALUE to validate the performance of the transfer functions .

Metric	Units
Relative Bias (for the mean, RB)	%
Relative Bias (for the 98th percentile, RBp98)	%
Root mean square error (RMSE)	mm·day^{-1}
Spearman correlation	-
ROC skill score (ROCSS)	-
Bias (median wet annual max spell, WetAMS)	day
Bias (median dry annual max spell, DryAMS)	day
Bias (relative amplitude of annual cycle, RAAC)	-

3.5 Repeatability

Achieving *repeatability* is a fundamental target of the present study. Repeatability is a known issue for calculations carried out on GPU systems (Jézéquel et al., 2015; Nagarajan et al., 2018; Alahmari et al., 2020) due to non-deterministic algorithm implementations and also for climate science in general (Bush et al., 2020). This issue intensifies when several components of the computation change, such as hardware, software and driver versions. Also, Nagarajan et al. (2018) identified several sources of *non-determinism*, which we aimed to comply with.

Three measures were taken in order to accomplish repeatability on the described hardware. First, a *Singularity container-ized environment* (Kurtzer et al., 2017) was created, which comprises all the needed software and drivers to train the transfer functions . Among the software included are `NVIDIA drivers 460.73`, `CUDA 11.2.1`, `CUDNN 8.1.0`, `R 3.6.3`, `Python 3.7.11`, `TensorFlow 2.5.0`, and the `climate4R` framework, using `Ubuntu 18.04.5 LTS` as base image. The second measure includes the *seeding* of the random numbers of the modules that interface with the GPU internal work, `NumPy`, `random` and `TensorFlow`, for `Python` from `R`, using the `reticulate` package (Allaire et al., 2017). And lastly, we used the recent deterministic implementation of algorithms that were past sources of GPU non-determinism via the flag `TF_DETERMINISTIC_OPS=1` (NVIDIA, 2021), which reportedly guarantees determinism under same number of GPUs, GPU architecture, driver version, `CUDA` version, `CUDNN` version, framework version, distribution set-up and batch size (Riach, 2021). Most of the calculations were carried out on a single A-100 GPU, yet, multi-GPU is fully supported by the *container* and the code, but was not thoroughly tested. The container is hosted on *Zenodo* (Quesada-Chacón, 2021a).

For each combination of number of layers, activation functions for both inside the *U* structures and last *ConvUnit*, spatial drop-out ratio, number of starting feature channels, number of feature channels for the last *ConvUnit*, and batch normalizations ten different runs, each with a different *seed number*, were carried out in order to find or approximate the global minimum

of their loss functions. A case scenario was added, where high-performing transfer functions were repeated ten times under the exact same *seed* and configuration to analyse the repeatability capabilities of the hereby introduced container and overall workflow. The influence of the deterministic operations on the runs were examined.

4   Results and discussion

4.1   Transfer function performance

Due to the experimental nature of deep learning and the great number (thousands) of possible configuration combinations, several iterations were needed to narrow down which *hyperparameters* significantly improved the performance of the transfer functions , which were superfluous and which should be further tested. The following results show the last iteration of this approach under *deterministic* conditions. Along this trial and error process some *hyperparameters* were fixed, i.e., *leaky ReLu* as general activation function, *spatial drop-out* ratio of 0.25 and *batch normalization* of the weights inside the *U* structures, no *spatial drop-out* for the *ConvUnit* after the *U* architectures, *learning rate* of 0.0005 for the *Adam* optimizer, a *patience* of 75 epochs with a maximum of 5000 epochs, with the `save_best_only = TRUE` option set, and a *batch size* of 512.

The *hyperparameters* explored in the last iteration are then: *U-Net* and *U-Net++* architectures; number of layers of the *U* structures (i.e., 3, 4 and 5); number of starting *features* of the *U* structures (16, 32, 64 and 128), which doubles on each layer; number of *channels* of the *ConvUnit* after the *U* architecture, 1 and 3 (the rationale being one per each of the *Bernoulli Gamma* distribution parameters); and both the `TRUE` and `FALSE` possibilities for the *batch normalization* of the aforementioned *ConvUnit*. The previous parameters, in the mentioned order, were used to create a nomenclature to ease the readability of the models, e.g. *Upp-4-64-3-F* means that the model was trained under a *U-Net++* architecture with 4 layers, where the first one had 64 filters, ending with a *ConvUnit* with 3 channels and no *batch normalization*.

Remarkably, the "original" initial number of *feature channels* for the *U*-like architectures is 32, which were mostly used in gray-scale (one input channel) or RGB (three input channels) image processing tasks. In the current assignment 20 input channels (the predictors) are present, which was the rationale behind adding 64 and 128 initial *feature channels*. Some of the predictors might be collinear, thus testing the original 32 and adding 16 filters as counterpart was key to assess the performance.

The resulting combinations of the preceding *hyperparameters* coupled with *CNN1* and the three other similar models (*CNN32-1*, *CNN64-1* and *CNN64_3-1*) amounts to 100 different ones, which were trained under ten different *random seed numbers*, for a grand total of 1000 trained models. Since each *seed* represents a different "starting point" on the loss function topology, which increases in complexity with larger numbers of parameters, divergent performance for the same architecture under various *seeds* is foreseeable.

The metrics shown in Table 1 were computed for the independent validation dataset (2010-2015). The performance of each metric per individual model was ranked, and then the sum of all the individual ranks was employed to obtain an overall rank. Also, it was observed that for 297 transfer functions at least one pixel was returning *not real numbers*, therefore, these models were excluded from the analysis, although the reasons behind their "failure" are discussed later on. After reviewing the resulting ranking, it was noticed that some of the metrics of the best performing models were not satisfactory, e.g. high ROCSS

and Spearman correlation but poor performance of the spells, WetAMS and DryAMS, the latter being the most challenging
metric to accurately model. Therefore, to short-list and decide which models to select, the conditions shown in Table 2 were
applied to the median validation metrics, which reduced the number of transfer functions that complied to 35.

Table 2. Conditions applied to the median validation metric values of the transfer functions for further pruning.

Lower threshold		Metric		Upper threshold	Units
-3	$\leq$	RB	$\leq$	3	%
-10	$\leq$	RBp98Sto	$\leq$	10	%
-10	$\leq$	RAAC	$\leq$	10	-
-1	$\leq$	WetAMS	$\leq$	1	day
-1.5	$\leq$	DryAMS	$\leq$	1.5	day

After implementing the aforementioned conditions, the best *CNN1* (none of the 10 runs complied) and the best eleven
performing architectures were selected and further analysed, i.e., duplicated architectures like *U-3-64-1-T* (overally ranked #2
and #11) and *Upp-3-64-1-F* (#3 and #20) were removed to show the performance of different ones. Boxplots of the validation
performance metrics of selected models are shown in Figure 3.

In general, the performance of the *U-like* models exceed the one of the benchmark, *CNN1*, for most of the metrics with
respect to both the median and the variability of the results. Note that the best run of *CNN1* is ranked #484 out of the remaining
703 models. *DryAMS* is the major weakness for *CNN1*, yet ROCSS, Spearman correlation and RMSE are also unsatisfactory,
which are key to the overall performance. Also, the variability of the RB-based metrics and RMSE is quite large compared to
most of the other models, as shown by the span of the whiskers.

Particularly, the #1 ranked model, *Upp-4-128-3-F*, was initially excluded from the analysis because of its high DryAMS
bias (see the unpruned analogous to Figure 3 in Figure A1). Further examination revealed that the variability of its metrics is
considerably higher than for other models and only 3 out of the 10 runs of this architecture did not end as "failures", so that
this particular exceptional performance could have been a matter of happenstance rather than the architecture being optimal
for the task.

It is worth noting that *CNN1* comprises 5,912,251 parameters while ranked #2 architecture *U-3-64-1-T* and ranked #3 archi-
tecture *Upp-3-64-1-F* include 7,769,465 and 7,950,389 parameters, respectively. This reaffirms the performance improvement
induced by the skip connections with a rather minor proportional increase in the number of parameters. However, the robustness
provided by both architectures takes around three- and fourfold training time per step (20 steps per epoch for all the models),
respectively, which sums up to between five- and sevenfold the total training time for #2 and #3 (see Table 3).

Additionally, in the training–validation loss plots for *CNN1* (see Figure A2) it was observed that shortly after reaching the
minimum, the validation loss curve started to diverge from the training loss one, which can be interpreted as overfitting of the
model and explains the relative small number of epochs needed during training, due to the *patience* set. This behaviour was not
observed for the *U*-like architectures or is at least not so evident as for *CNN1*. Still, since only the best model per architecture
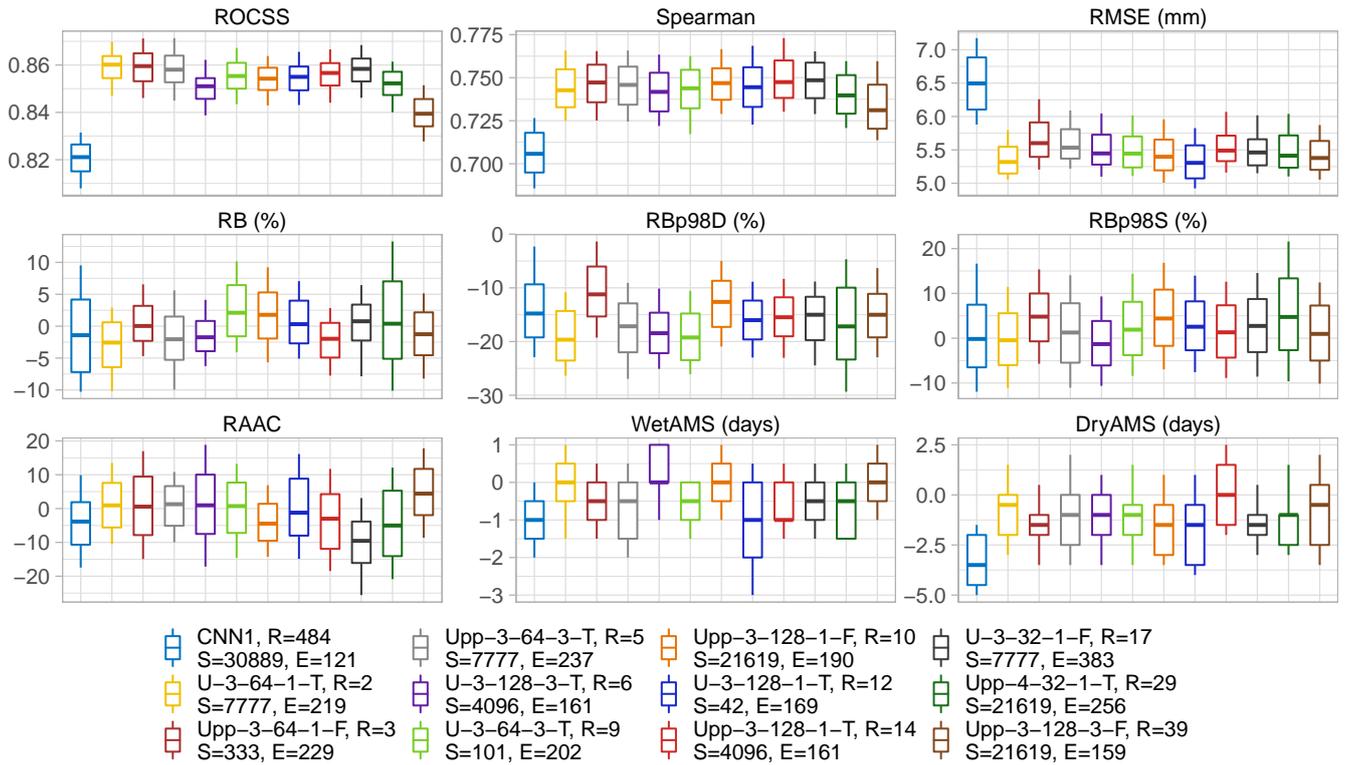
Figure 3. Validation metrics of *CNN1* (benchmark) and the eleven best performing architectures after pruning, ordered according to their rankings. Each sub-panel contains 12 boxplots, one per model, which summarises the results for the 1916 pixels within the Eastern Ore Mountains. The boxes comprise the 25th and 75th percentile as well as the median, the whiskers the 10th and 90th percentile. The letters *D* and *S* after *RBp98* stand for deterministic and stochastic approaches, respectively. Note that in the legend, ordered column-wise, alongside the nomenclature of the models details are added such as the overall ranking (*R*), the *random seed number* (*S*) of the run and the number of epochs (*E*) needed to train the transfer functions (due to the *patience* of 75, the shown performance was achieved in *E*-75 epochs).

was saved during training before *early stopping*, the performance metrics were not compromised, yet, the model architecture might not be ideal for the task at hand.

The model ranked #2 (*U-3-64-1-T*) is considerably superior to the other ones with respect to most of the validation metrics. This includes the lower variance for most of the variables and a clear advantage on RMSE and the spells (-0.5 median value for both), which were a rather hard task for most of the models and are key performance metrics for potential subsequent impact modelling use of the downscaling output.

Noticeably, the RBp98, under a *deterministic* approach, is the metric with the poorest behaviour overall, which is between -10% and -20% for most of the transfer functions . This could be explained by the joint effect of the already shown RB in Figure 1a and the extreme events of 2013, included in the independent validation metrics calculation only. Nevertheless, the stochastic approach shows a satisfactory performance, although it should be used carefully, since the temporal and spatial

Table 3. Computational details of some of the models. Note that some models not shown before, like *Upp-5-128-3-T*, which was the largest model trained, are added for completeness. All the following calculations were carried out on a NVIDIA A-100 (40 GB) GPU, with a batch size of 512, resulting in 20 steps per epoch. The table is ordered according to the ascending number of total parameters in the models.

Model	Para-meters	Seed	Rank	Epochs	ms/step	Total time (s)
CNN1	5.91 M	30889	484	121	27	62.9
U-3-16-1-F	6.01 M	42	102	423	43	363.8
U-3-32-1-F	6.37 M	7777	17	383	51	390.7
U-3-64-1-T	7.77 M	7777	2	219	74	324.1
U-5-16-1-F	7.84 M	101	364	264	50	264.0
Upp-3-64-1-F	7.95 M	333	3	229	98	448.8
Upp-4-32-1-T	8.11 M	21619	29	256	95	486.4
U-4-64-1-T	13.61 M	31	48	158	86	271.8
Upp-4-64-1-T	14.73 M	42	158	185	147	543.9
Upp-3-64-3-T	19.72 M	7777	5	237	99	469.3
U-3-128-3-T	25.14 M	4096	6	161	140	450.8
U-5-64-1-T	42.09 M	21619	271	131	215	563.3
Upp-4-128-3-F	52.96 M	30889	1	135	303	818.1
Upp-5-64-3-T	53.86 M	11	398	140	211	590.8
Upp-5-128-3-T	162.35 M	7777	284	156	467	1 457.0

structure is lost due to its underlying logic (Baño-Medina et al., 2020), as observed in the RBp98S row of Figure 4. Therefore, longer-term averages and/or aggregated regions would be an appropriate use case for the datasets generated under this procedure.

The first six models shown in Figure 3 were chosen to further assess the spatial distribution of the metrics, as shown in Figure 4. Both ROCSS and Spearman correlation have a rather smooth spatial distribution of their values, with a noticeable decrease in its performance in the south-eastern corner of the region for all the models, as seen in Figure 4. The median RB of *CNN1* is -1.42%, but its high variability can be noticed, particularly towards the north-west of the Eastern Ore Mountains, while e.g. #2 (median -2.57%) shows a smoother distribution. The median RB of *U-3-64-3-T* is better than for #2 but has a noisier behaviour, which depending on the application of the downscaled datasets, could play an important role.

In case of RBp98 under deterministic conditions, *Upp-3-64-1-F* has the best overall results with intermediate variability. Generally, smoother contrasts are seen for the *U*-like models for most of the metrics. RAAC shows high spatially distributed discrepancies, particularly for *U-3-128-3-T* and *U-3-64-3-T*, with very low values in the north-west and intense positive deviations in the south-east. Smaller but consistent differences are seen for most of the models.

During the analysis it was evident that the "full size" of the *U*-like architectures, five layers, did not provide the best performance, which in computer vision assignments tends to excel. This finding could be partially explained by the relative
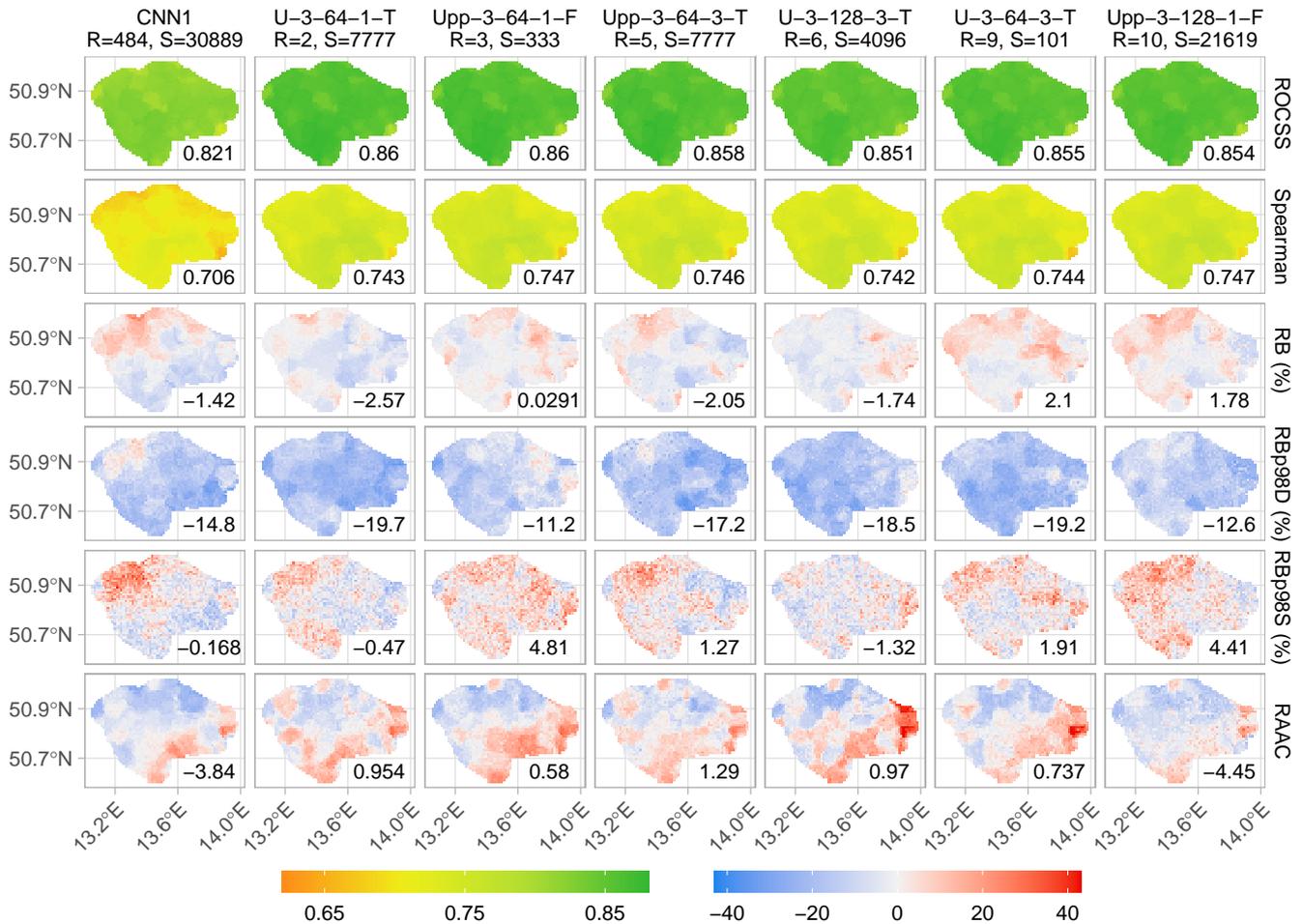
Figure 4. Spatially distributed validation metrics, row-wise, of *CNN1* (benchmark) and a sub-selection of the best performing models. The numbers inside the panels represent the overall median of the metrics amongst the Eastern Ore Mountains domain. Note the shared scales among the metrics.

small size of the domain, 32 by 32 pixels. Because of the domain side halving logic enforced by these architectures on each layer, joint with the lack of extra `padding`, the remaining domain size in the fifth layer was only 2 by 2, which possibly limits the efficiency of the models. Also, *overfitting* might have played a significant role ruling out the larger models. Generally, the smaller models achieved better performances, which could change with a larger predictor domain size, e.g. 64 by 64.

Furthermore, it seems that the starting point in the *loss function* topology plays a significant role in the transfer function performance, particularly under the *early stopping* settings used. Therefore, further assessments of the balance between the number of different seeds numbers, early stopping and total calculation time should be carried out for similar future applications, in order to optimize GPU time use. With the same purpose in mind, *batch size* could be programmed to be a transfer function dependent number for GPU memory use optimization.

Regarding the transfer functions that resulted in non-real numbers in at least one pixel of the whole domain (297 cases), a couple of noteworthy details were found. First, the type of *U* architecture and number of initial *channels* did not seem to be a decisive factor: 153 were *U-Net* and 144 *U-Net++*. This small difference could be explained due to the added robustness of the additional skip connections given by the latter architecure. Furthermore, 84, 87, 71 and 55 "failed" transfer functions were related to models with 16, 32, 64 and 128 initial feature channels, respectively. The *random seed number* or "starting point" appears to have considerable influence on the "failed" models: `seed=11` is related to 36 failures, while the most successful one had 22 (`seed=7777`). Table 4 is shown to better understand the influence of some hyperparameters on the failure of the models.

Table 4. Grouping of the transfer functions resulting in *non-real number* values in at least one pixel in the Eastern Ore Mountains domain, according to number of filters in the last *ConvUnit* and batch normalization condition.

Filters last *ConvUnit*	Batch Normalization	Count
1	TRUE	1
1	FALSE	10
3	TRUE	117
3	FALSE	169

Note that only one model corresponds to the combination of one feature channel on the last *ConvUnit* with *batch normalization* and ten without it, which could mean that the extra parameters (3 channels) on the last layer add noise to the model that results more frequently in non-real values. Furthermore, not applying batch normalization to the last *ConvUnit* leads to a greater number of failures (179 versus 118). Therefore, it is suggested for subsequent studies to use batch normalization with a single channel on the last layer. Models with larger numbers of layers and initial channels (see Table A1 and Table A2), and therefore larger total numbers of parameters, tend to "fail" with the independent validation dataset more often than the smaller ones, probably due to overfitting. Combinations of three filters in the last *ConvUnit* with no batch normalization "failed" more often than their normalized counterparts, and this behaviour augmented with the number of layers of the *U-like* architectures. Furthermore, a lower number of initial channels (16 and 32) tends to "fail" more often and this behaviour increases with the depth of the *U-like* structure. This "failure" probably happens when the transfer function can not handle unseen conditions during training (lack of extrapolation capability) and is related to hyperparameters that form a more "rugged" loss function topology, permitting under- and overfitting of the models.

4.2 Repeatability

As mentioned previously, general reproducibility is a notorious issue for both climate science and GPU based calculations. In addition, deep learning techniques are not yet completely approved by the climate community, mostly due to interpretability concerns, deepened by the general reproducibility ones. Therefore, attempting to provide a repeatable framework was a cornerstone enterprise of the study while being aware of the properties and limitations of both the hardware and software. Thus,

Figure 5 presents the experiment described in subsection 3.5, showing five of the validation metrics and the minimum *Bernoulli*
350   *Gamma* loss function value from the ten different runs for the benchmark *CNN1*, and the models ranked #2 to #3 under both
deterministic and non-deterministic conditions.
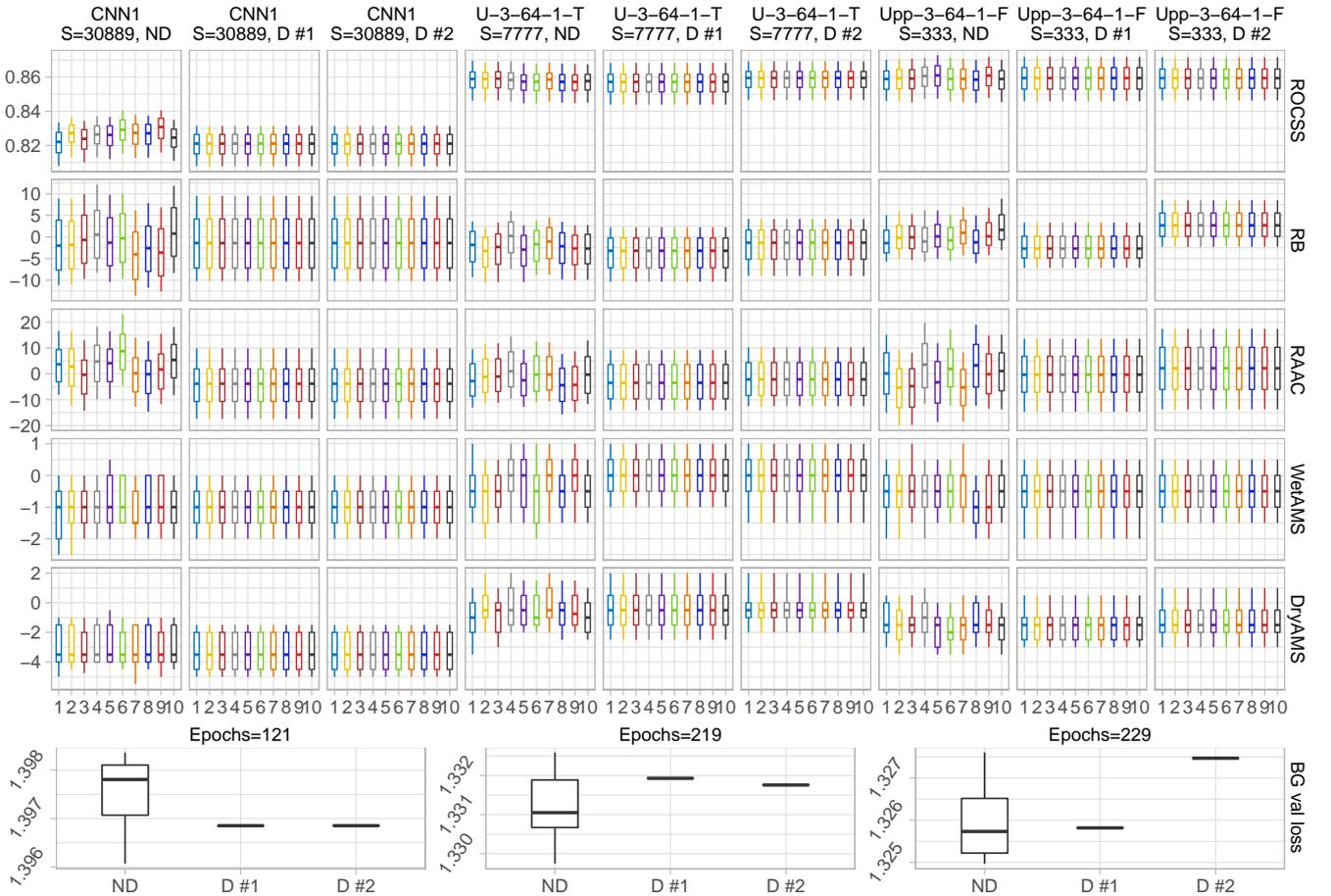
Figure 5. Comparison among ten runs under the same *seed number* and configuration for the benchmark and a sub-selection of the best
performing transfer functions ordered column-wise. A sub-selection of the metrics from Table 1 is shown row-wise plus a row which depicts
the boxplots of the minimum value achieved by the Bernoulli Gamma loss function (BG val loss) during training per type of run and model.
D stands for deterministic and *ND* for non-deterministic runs. Note that all the runs per model needed the same amount of epochs.

As noticeable from Figure 5, all the ten deterministic runs of the same model result, as expected, in the exact same outcome.
Thus, *repeatability* was achieved. Yet, depending on which specific GPU out of the 272 same ones available in *Alpha Centauri*
is used, minor differences can be observed among them, despite complying with the conditions that reportedly guarantee
355   determinism (see subsection 3.5). Both deterministic repetitions for *CNN1* were done on the same physical GPU, therefore,
all of the 20 runs resulted in the exact same value for all metrics and pixels. In the case of the repetitions for *U-3-64-1-T* and
Upp-3-64-1-F, which were trained on different physical GPUs of the same sub-cluster (same hardware) using the same source

code and container, minor variations among them were observed, which can be interpreted as the aforementioned *similarity*. Despite not being able to exactly repeat the outcomes under different GPUs, the hereby presented results are quite satisfactory for the scope of this project.

From the non-deterministic runs shown in Figure 5 it can also be observed that the variability of the results was considerably narrowed down, through the *containerization* of the environment and the *seeding* of the random numbers, which can also be interpreted as a measure of *similarity*. The latter can be seen in the last row of the aforementioned figure, where e.g. the minimum in-training *Bernoulli Gamma* validation loss function for the different configurations start to differ in the third or fourth decimal place. Nevertheless, strong variations are observed within the different runs per model, which might lead to some runs having a substantial better performance than the remaining ones without a foreseeable reason rather than randomness and non-determinism. Lastly, it is worth noting that the non-deterministic runs were calculated faster, e.g. 23 ms/step instead of 27 for *CNN1*, 71 instead of 74 for *U-3-64-1-T* and 90 instead of 98 for *Upp-3-64-1-F*.

4.3   Suitability of the architectures

The deterministic results presented in subsection 4.2 constitute the last iteration of the present project. However, before achieving this cornerstone, non-deterministic operations were employed and several noteworthy details regarding the suitability of the architectures for this particular task were found, which we believe deserve a place in the present discussion. Figure 6 shows a sub-selection of transfer functions chosen to illustrate some of these features.

Initially, it can be observed that some runs of the same architecture needed different number of epochs to train, categorized in one to four scenarios, in contrast to the results shown in Figure 5. We believe that the number of training scenarios can be interpreted as a measure of model suitability or of how rugged its loss function topology is, which is in turn related to under- or overfitting of the models (see Figure A2). A lower number of scenarios under non-deterministic conditions implies that the inherent noise is to a certain extent suppressed. In the case of *CNN1* for `seed=4096`, three scenarios were identified with 112 epochs being clearly the best performing one. Three out of the ten runs fell into this scenario (1, 4 and 7), which confirms that depending of the architecture, the best result might be a matter of randomness. The same behaviour can be observed for other architectures with multiple training scenarios and can be interpreted as a measure of *dissimilarity*.

Notably, the hyperparameters mentioned in subsection 4.1, which did not result in non-real values (i.e., batch normalization, three or four layers, just one channel in the last *ConvUnit*, and 64 or 128 initial feature channels) are the ones that generally lead towards a more stable or smooth loss function, which in turn may reduce the number of training scenarios under non-deterministic conditions, producing *similar* outcomes. On the other hand, the 16 initial filters and no batch normalization of *Upp-3-16-1-F* might result in a rather rugged loss function topology. The aforementioned architecture produced four different training epochs scenarios, which decrease its suitability and similarity. Thus, for the specific conditions of the present task, the combination of 3 layers with either 64 and 128 filters, or 4 layers with 64 filters, one channel and batch normalization in the last *ConvUnit* for both *U-like* models, is the *sweet-spot* for the architecture suitability.
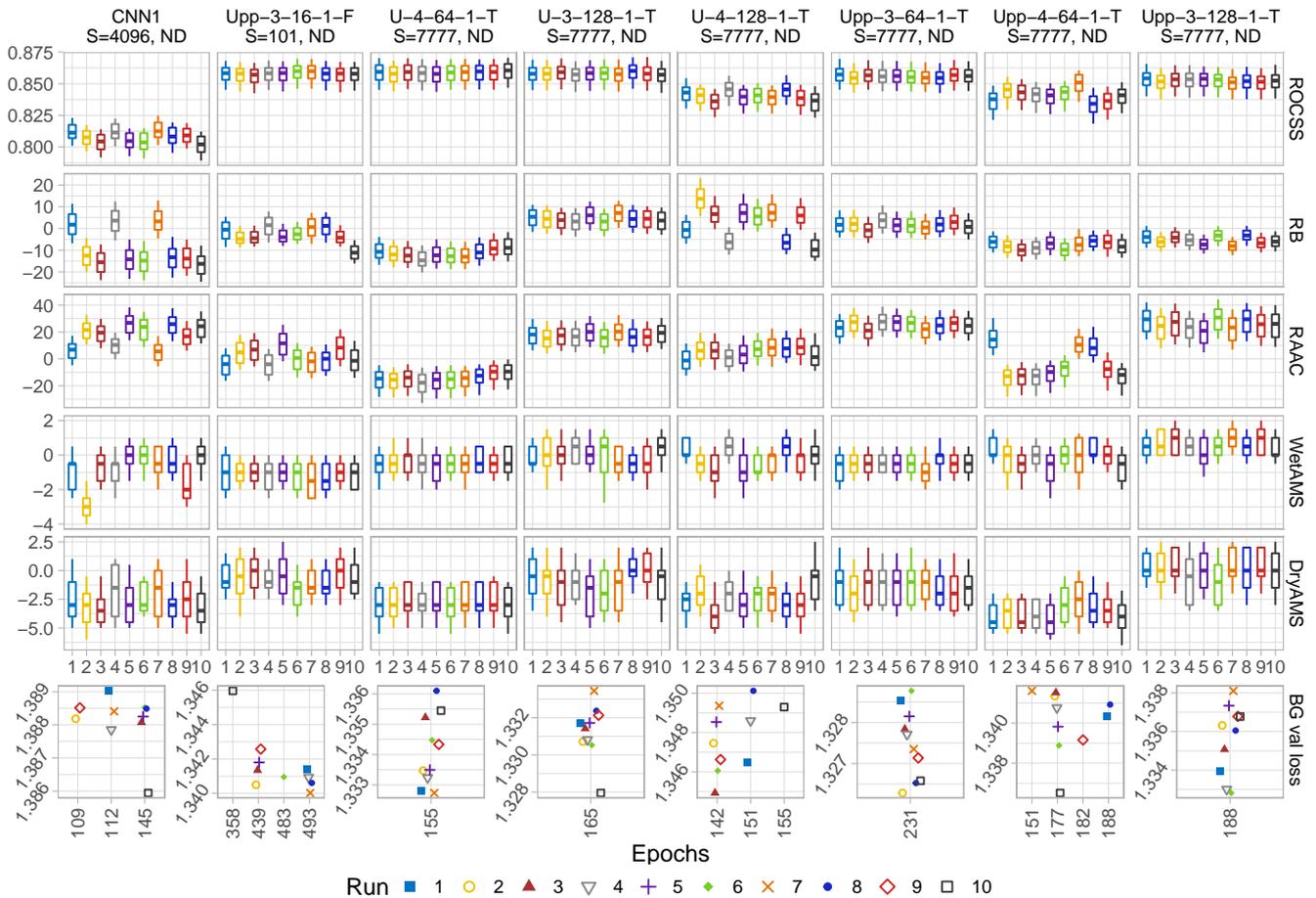
Figure 6. Similar to Figure 5 but for other architectures under non-deterministic conditions only. The last row depicts the minimum value achieved by the Bernoulli Gamma loss function (BG val loss) during training and the number of epochs needed to train the models. Note that the *x-axis* of the last row is not to scale and the symbols are avoiding other ones on similar positions to ease its readability, thus, refer to the closest abscissa grid-line to interpret its epoch.

5 Summary and outlook

Deep learning methods have substantially developed over recent years in various domains, with computer vision studies focused on medical imaging often being pioneers. However, there are still interpretability concerns with deep learning models and well-known general reproducibility issues with GPU accelerated calculations (Jézéquel et al., 2015; Nagarajan et al., 2018; Alahmari et al., 2020). Nevertheless, there are various recent studies including algorithms such as CNNs for statistical downscaling applications with promising outcomes, Baño-Medina et al. (2020) being the benchmark for the present study. However, the aforementioned study did not include recent architectures such as *U-Net* and *U-Net++* nor GPU accelerated calculations.

Considering the costs of developing worldwide physically based projections on an impact-model-relevant scale, and the urgency with which this information is required, we therefore focused our efforts on improving the building blocks to use deep learning towards repeatable high-resolution statistical downscaling, particularly with a methodology extendable to other regions, spatio-temporal scales and diverse variables while taking advantage of state-of-the-art architectures and hardware.

A *hyperparameter-space* search including one hundred distinct models was carried out applying ten different seed numbers to examine their optimum values and patterns in both performance and repeatability terms. In general, the skip connections based models performed significantly better than the best run of the benchmark *CNN1* in both median and variability terms for the performance metrics taken from the *VALUE* framework. *U-3-64-1-T* was the overall best performing model for the present arrangement, considering the configuration of input channels and numbers of input and output pixels, which consist of 3 layers with 64, 128 and 256 feature channels, respectively, and a single channel with batch normalization on the convolutional layer after the *U-Net* structure. The latter is in terms of deep learning a rather simple model. Its total number of parameters is 7.77 million, which in contrast to the 5.91 million parameters of *CNN1*, represents a strong improvement without major computing requirements. The total training time for the aforementioned model was approximately six minutes with one NVIDIA A-100 GPU, under the shown configuration.

The hereby presented workflow demonstrated satisfactory performance to downscale daily precipitation using as predictors 20 variables of the *ERA5* reanalysis to a resolution of 1 km, offered by the *ReKIS* dataset. Though the method is in principle able to work with station data, too, benefiting from spatially distributed predictors, its clear advantage are the result fields e.g. needed for impact modelling with lateral exchange like hydrological modelling. Besides the here applied geostatistical product ReKIS, e.g. in regions or for variables with less dense measurement networks, regional reanalysis products like *COSMO-REA2* (Wahl et al., 2017) can be employed. The outcomes of the method were validated through the robust *VALUE* framework, while building upon the climate4R structure, which due to the reach of R in several related fields, could prove greatly beneficial for further associated and/or derived studies.

Furthermore, the presented transfer functions, as well as other ones to be derived for additional variables, will be applied to the EURO-CORDEX 0.11° ensemble. The latter offers a greater amount of GCM-RCM combinations and variables than EURO-CORDEX 0.22°. Thus, a rather straightforward upsampling method could be enough to match the EURO-CORDEX 0.11° and ERA5 grids. The projections for the Eastern Ore Mountains are then intended to serve as input to multi-purpose impact models, such as hydrological, agronomic and ecological ones.

The *Singularity* container developed for the present task allowed further scrutiny of the GPU deterministic implementations, repeatability capabilities and the suitability of the different architectures tested. Full repeatability was achieved when using the exact same physical GPU. A high degree of similarity was accomplished among runs on different GPUs, even though we complied with the reported conditions for repeatability, hardware- and software-wise. Still, this is a highly satisfying outcome. The models were trained on state-of-the-art hardware (*Alpha Centauri* sub-cluster), nevertheless, they can be recalculated, with the corresponding adjustments in e.g. batch size and subsequent learning rate changes, on alternative GPU models or on CPU.

The presented approach addresses the underlying *general reproducibility* issues while complying with the conditions for *methods reproducibility* (Goodman et al., 2016). The achieved repeatability is essential to build trust in deep learning applica-

tions and to further develop towards interpretable models. The latter is particularly relevant for statistical downscaling, where interpretability of the transfer functions is fundamental to trustfully downscale projected climate change scenarios.

Code and data availability. The processed predictors and predictand used for the development of the models can be found in https://doi. org/10.5281/zenodo.5809553 (Quesada-Chacón, 2021b). The *singularity container* used for the calculations can be downloaded at https: //doi.org/10.5281/zenodo.5809705 (Quesada-Chacón, 2021a). The version of the code employed in this paper can be found at https://doi.org/ 10.5281/zenodo.5856118 (Quesada-Chacón, 2022a). The repository https://github.com/dquesadacr/Rep_SDDL (Quesada-Chacón, 2022b) hosts the rendered description of the software with further details to properly run and modify the source code.

435
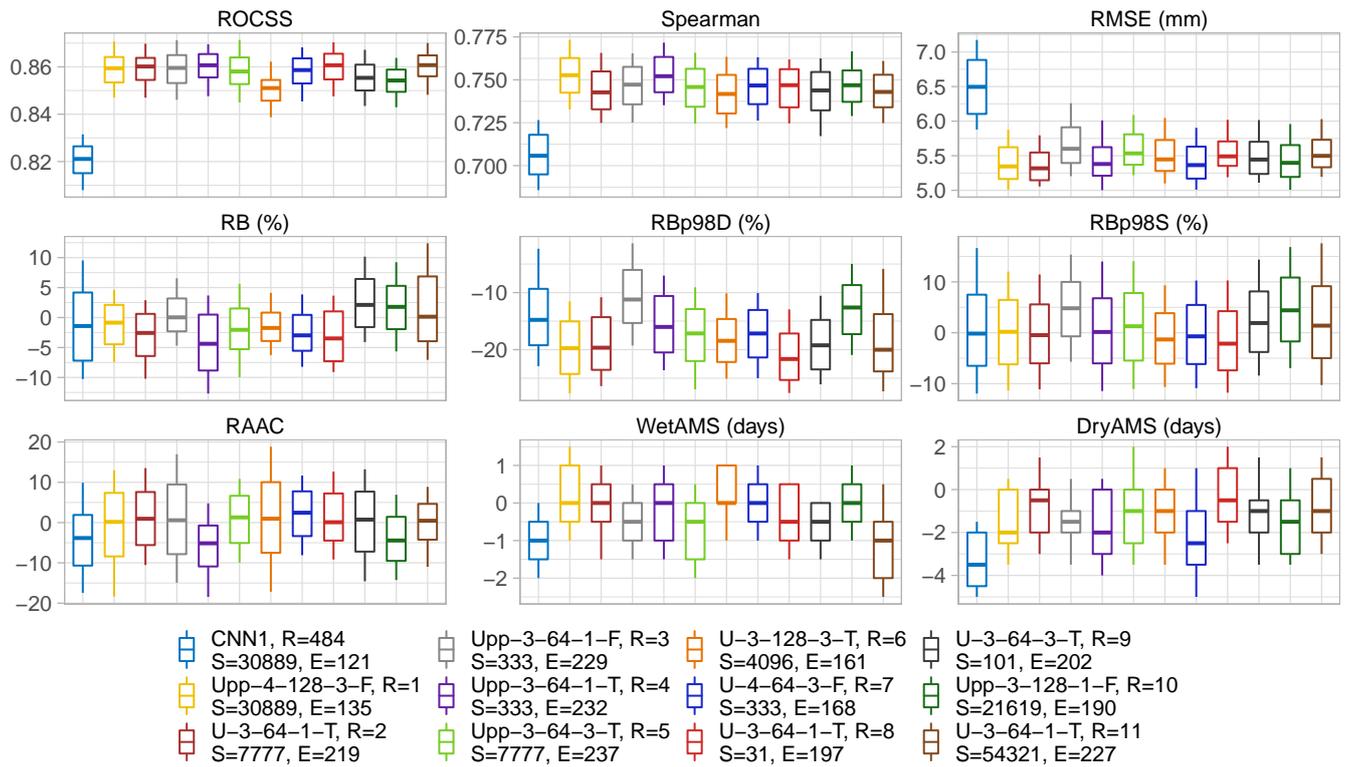
Figure A1. Same as Figure 3 but without the filtering conditions applied.
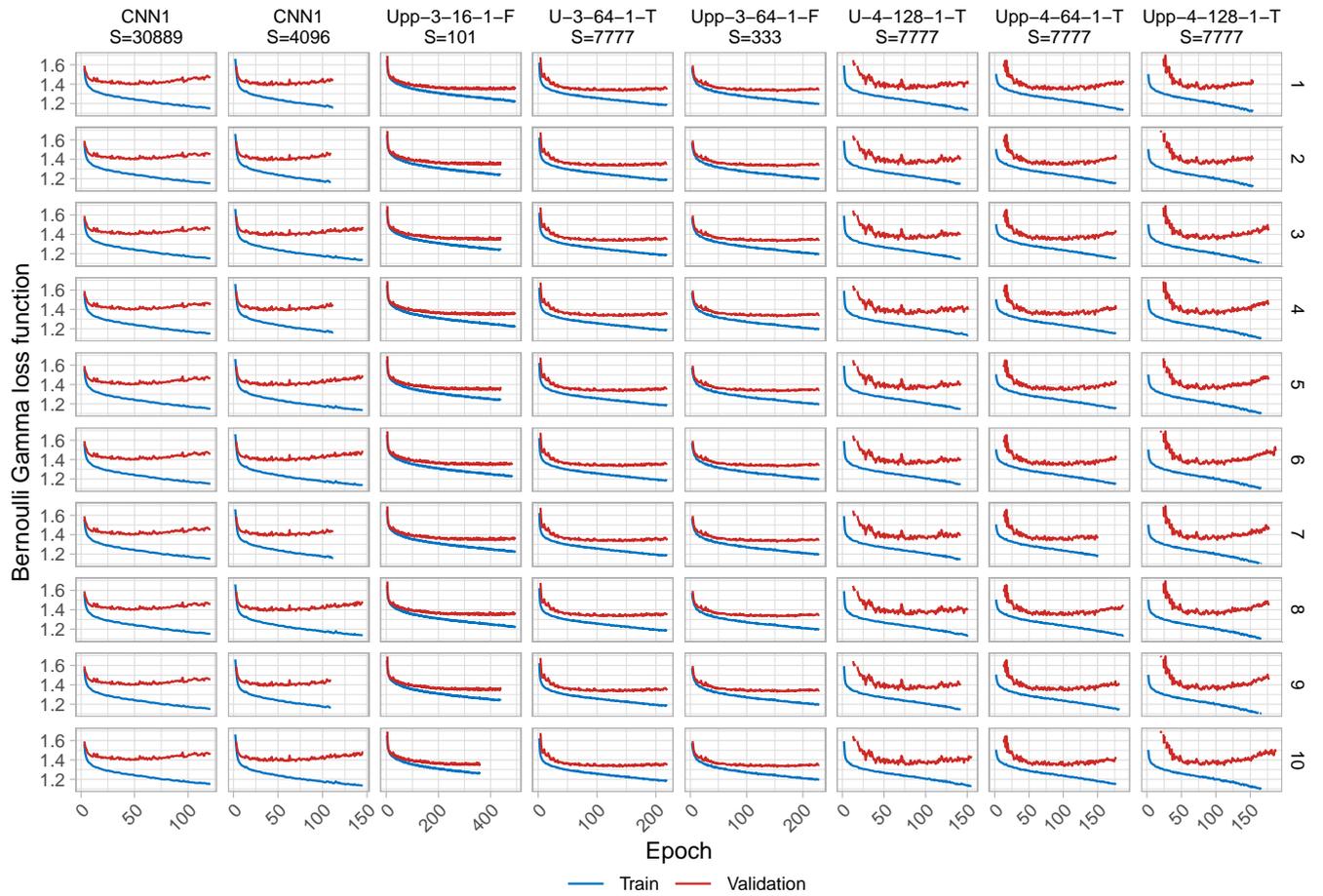
Figure A2. Training-validation loss plots for ten runs under the same *random seed number* and configuration for the benchmark and a sub-selection of the transfer functions under *non-deterministic* conditions, ordered column-wise.

Table A1. Similar to Table 4 but grouped according to amount of *layers*, *filters* in the last *ConvUnit* and *batch normalization*.

Layers	Filters last *ConvUnit*	Batch Normalization	Count
3	1	TRUE	0
3	1	FALSE	1
3	3	TRUE	22
3	3	FALSE	32
4	1	TRUE	0
4	1	FALSE	3
4	3	TRUE	42
4	3	FALSE	60
5	1	TRUE	1
5	1	FALSE	6
5	3	TRUE	53
5	3	FALSE	77

Table A2. Similar to Table 4 but grouped according to amount of *layers*, *filters* in the last *ConvUnit* and *initial feature channels*.

Layers	Filters last *ConvUnit*	Initial Channels	Count
3	1	16	1
3	1	32	0
3	1	64	0
3	1	128	0
3	3	16	16
3	3	32	21
3	3	64	22
3	3	128	6
4	1	16	2
4	1	32	1
4	1	64	0
4	1	128	0
4	3	16	26
4	3	32	29
4	3	64	25
4	3	128	22
5	1	16	2
5	1	32	3
5	1	64	1
5	1	128	1
5	3	16	37
5	3	32	33
5	3	64	34
5	3	128	26

Author contributions. All authors conceptualised the study and the grant proposal. DQC preprocessed the input data, planned the methodological approach and experiments, wrote the code, built the container, generated the results and figures, analysed the results, and wrote the draft. All authors revised and approved the manuscript.

Competing interests. The authors declare that they have no conflict of interest.

Acknowledgements. We want to thank: the Santander Meteorology Group for providing the `climate4R` tools and related papers on which this study is built upon, particularly Dr. Jorge Baño-Medina for his kind availability to discuss his work, the European Centre for Medium-Range Weather Forecasts (ECMWF) for providing the ERA5 reanalysis data, the Regionales Klimainformationssystem (ReKIS) for the gridded precipitation data, and Dr. Peter Steinbach from Helmholtz-Zentrum Dresden-Rossendorf (HZDR) for valuable comments on the manuscript. We appreciate the generous allocations of compute resources by the Center for Information Services and High Performance Computing (ZIH) of the Technische Universität Dresden and the support of the Competence Center for Scalable Data Services and Solutions Dresden/Leipzig (ScaDS). The authors and the editor thank two anonymous reviewers whose comments improved the presentation of this manuscript.

Financial support. This research is funded by the European Social Fund and co-financed by tax funds based on the budget approved by the members of the Saxon State Parliament (100380876).

References

Abadi, M., Agarwal, A., Barham, P., Brevdo, E., Chen, Z., Citro, C., Corrado, G. S., Davis, A., Dean, J., Devin, M., Ghemawat, S., Good-fellow, I. J., Harp, A., Irving, G., Isard, M., Jia, Y., Józefowicz, R., Kaiser, L., Kudlur, M., Levenberg, J., Mané, D., Monga, R., Moore, S., Murray, D. G., Olah, C., Schuster, M., Shlens, J., Steiner, B., Sutskever, I., Talwar, K., Tucker, P. A., Vanhoucke, V., Vasudevan, V., Viégas, F. B., Vinyals, O., Warden, P., Wattenberg, M., Wicke, M., Yu, Y., and Zheng, X.: TensorFlow: Large-Scale Machine Learning on Heterogeneous Systems, https://www.tensorflow.org/, software available from tensorflow.org, 2015.

Alahmari, S. S., Goldgof, D. B., Mouton, P. R., and Hall, L. O.: Challenges for the Repeatability of Deep Learning Models, IEEE Access, 8, 211 860–211 868, https://doi.org/10.1109/ACCESS.2020.3039833, 2020.

Allaire, J. J., Ushey, K., Tang, Y., and Eddelbuettel, D.: reticulate: R Interface to Python, https://github.com/rstudio/reticulate, 2017.

Association for Computing Machinery (ACM): Artifact Review and Badging Version 2.0, https://www.acm.org/publications/policies/artifact-review-badging, 2021.

Baño-Medina, J., Manzanas, R., and Gutierrez, J. M.: Configuration and intercomparison of deep learning neural models for statistical downscaling, Geoscientific Model Development, 13, 2109–2124, https://doi.org/10.5194/gmd-13-2109-2020, 2020.

Bastian, O., Syrbe, R. U., Slavik, J., Moravec, J., Louda, J., Kochan, B., Kochan, N., Stutzriemer, S., and Berens, A.: Ecosystem services of characteristic biotope types in the Ore Mountains (Germany/Czech Republic), International Journal of Biodiversity Science, Ecosystem Services and Management, 13, 51–71, https://doi.org/10.1080/21513732.2016.1248865, 2017.

Bush, R., Dutton, A., Evans, M., Loft, R., and Schmidt, G. A.: Perspectives on Data Reproducibility and Replicability in Paleoclimate and Climate Science, Harvard Data Science Review, 2, https://doi.org/10.1162/99608f92.00cd8f85, 2020.

Cannon, A. J.: Probabilistic multisite precipitation downscaling by an expanded Bernoulli-Gamma density network, Journal of Hydrometeorology, 9, 1284–1300, https://doi.org/10.1175/2008JHM960.1, 2008.

Cavazos, T. and Hewitson, B.: Performance of NCEP–NCAR reanalysis variables in statistical downscaling of daily precipitation, Climate Research, 28, 95–107, 2005.

Chollet, F. et al.: Keras, https://github.com/fchollet/keras, 2015.

CORDEX: CORDEX - ESGF data availability overview, http://is-enes-data.github.io/CORDEX_status.html, last access: 13 November 2021, 2021.

Deutsch, C. V.: Correcting for negative weights in ordinary kriging, Computers and Geosciences, 22, 765–773, https://doi.org/10.1016/0098-3004(96)00005-2, 1996.

Deutsch, C. V. and Journel, A. G.: GSLIB: Geostatistical Software Library and User's Guide. Second edition, Oxford University Press, 1998.

Flato, G., Marotzke, J., Abiodun, B., Braconnot, P., Chou, S., Collins, W., Cox, P., Driouech, F., Emori, S., Eyring, V., Forest, C., Gleckler, P., Guilyardi, É., Jakob, C., Kattsov, V., Reason, C., and Rummukainen, M.: Evaluation of climate models, in: Climate Change 2013 – The Physical Science Basis: Working Group I Contribution to the Fifth Assessment Report of the Intergovernmental Panel on Climate Change, pp. 741–866, Cambridge University Press, https://doi.org/10.1017/CBO9781107415324.020, 2013.

Goodman, S. N., Fanelli, D., and Ioannidis, J. P.: What does research reproducibility mean?, Science Translational Medicine, pp. 96–102, https://doi.org/10.1126/SCITRANSLMED.AAF5027, 2016.

Gutiérrez, J. M., Maraun, D., Widmann, M., Huth, R., Hertig, E., Benestad, R., Roessler, O., Wibig, J., Wilcke, R., Kotlarski, S., San Martín, D., Herrera, S., Bedia, J., Casanueva, A., Manzanas, R., Iturbide, M., Vrac, M., Dubrovsky, M., Ribalaygua, J., Pórtoles, J., Räty, O., Räisänen, J., Hingray, B., Raynaud, D., Casado, M. J., Ramos, P., Zerenner, T., Turco, M., Bosshard, T., Štěpánek, P., Bartholy, J.,

490   Pongracz, R., Keller, D. E., Fischer, A. M., Cardoso, R. M., Soares, P. M. M., Czernecki, B., and Pagé, C.: An intercomparison of a large ensemble of statistical downscaling methods over Europe: Results from the VALUE perfect predictor cross-validation experiment, International Journal of Climatology, 39, 3750–3785, https://doi.org/10.1002/joc.5462, 2019.

Hallett, J.: Climate change 2001: The scientific basis. Edited by J.T. Houghton, Y. Ding, D.J. Griggs, N. Noguer, P.J. van der Linden, D. Xiaosu, K. Maskell and C.A. Johnson. Contribution of Working Group I to the Third Assessment Report of the Intergovernmental
495   Panel on Climate Change, Cambridge University Press, Cambridge. 2001. 881 pp. ISBN 0521 01495 6., Quarterly Journal of the Royal Meteorological Society, 128, 1038–1039, https://doi.org/10.1002/qj.200212858119, 2002.

Harder, P., Jones, W., Lguensat, R., Bouabid, S., Fulton, J., Quesada-Chacón, D., Marcolongo, A., Stefanović, S., Rao, Y., Manshausen, P., and Watson-Parris, D.: NightVision: Generating Nighttime Satellite Imagery from Infra-Red Observations, CoRR, http://arxiv.org/abs/2011.07017, 2020.

500   He, X., Chaney, N. W., Schleiss, M., and Sheffield, J.: Spatial downscaling of precipitation using adaptable random forests, Water Resources Research, 52, 8217–8237, https://doi.org/10.1002/2016WR019034, 2016.

Hersbach, H., Bell, B., Berrisford, P., Hirahara, S., Horányi, A., Muñoz-Sabater, J., Nicolas, J., Peubey, C., Radu, R., Schepers, D., Simmons, A., Soci, C., Abdalla, S., Abellan, X., Balsamo, G., Bechtold, P., Biavati, G., Bidlot, J., Bonavita, M., De Chiara, G., Dahlgren, P., Dee, D., Diamantakis, M., Dragani, R., Flemming, J., Forbes, R., Fuentes, M., Geer, A., Haimberger, L., Healy, S., Hogan, R. J.,
505   Hólm, E., Janisková, M., Keeley, S., Laloyaux, P., Lopez, P., Lupu, C., Radnoti, G., de Rosnay, P., Rozum, I., Vamborg, F., Villaume, S., and Thépaut, J. N.: The ERA5 global reanalysis, Quarterly Journal of the Royal Meteorological Society, 146, 1999–2049, https://doi.org/10.1002/qj.3803, 2020.

Hewitson, B. and Crane, R.: Climate downscaling: techniques and application, Climate Research, 7, 85–95, 1996.

Höhlein, K., Kern, M., Hewson, T., and Westermann, R.: A comparative study of convolutional neural network models for wind field
510   downscaling, Meteorological Applications, 27, 1–31, https://doi.org/10.1002/met.1961, 2020.

IPCC: Climate Change 2021: The Physical Science Basis. Contribution of Working Group I to the Sixth Assessment Report of the Intergovernmental Panel on Climate Change [Masson-Delmotte, V., P. Zhai, A. Pirani, S.L. Connors, C. Péan, S. Berger, N. Caud, Y. Chen, L. Goldfarb, M.I. Gomis, M. Huang, K. Leitzell, E. Lonnoy, J.B.R. Matthews, T.K. Maycock, T. Waterfield, O. Yelekçi, R. Yu, and B. Zhou (eds.)], Cambridge University Press, Cambridge, United Kingdom and New York, NY, USA, https://doi.org/10.1017/9781009157896,
515   2021.

Iturbide, M., Bedia, J., Herrera, S., Baño-Medina, J., Fernández, J., Frías, M. D., Manzanas, R., San-Martín, D., Cimadevilla, E., Cofiño, A. S., and Gutiérrez, J. M.: The R-based climate4R open framework for reproducible climate data access and post-processing, Environmental Modelling & Software, 111, 42–54, https://doi.org/10.1016/j.envsoft.2018.09.009, 2019.

Jézéquel, F., Lamotte, J. L., and Saïd, I.: Estimation of numerical reproducibility on CPU and GPU, Proceedings of the 2015 Federated
520   Conference on Computer Science and Information Systems, FedCSIS 2015, 5, 675–680, https://doi.org/10.15439/2015F29, 2015.

Joint Committee for Guides in Metrology: International Vocabulary of Metrology – Basic and General Concepts and Associated Terms (VIM) 3rd Edition, English, pp. 1–127, https://www.nist.gov/system/files/documents/pml/div688/grp40/International-Vocabulary-of-Metrology.pdf, 2006.

Kingma, D. P. and Ba, J. L.: Adam: A method for stochastic optimization, 3rd International Conference on Learning Representations, ICLR
525   2015 - Conference Track Proceedings, pp. 1–15, 2015.

Kronenberg, R. and Bernhofer, C.: A method to adapt radar-derived precipitation fields for climatological applications, Meteorological Applications, 22, 636–649, https://doi.org/10.1002/met.1498, 2015.

Kurtzer, G. M., Sochat, V., and Bauer, M. W.: Singularity: Scientific containers for mobility of compute, PLoS ONE, 12, 1–20, https://doi.org/10.1371/journal.pone.0177459, 2017.

530 Li, H., Xu, Z., Taylor, G., Studer, C., and Goldstein, T.: Visualizing the loss landscape of neural nets, in: Advances in Neural Information Processing Systems, edited by Bengio, S., Wallach, H., Larochelle, H., Grauman, K., Cesa-Bianchi, N., and Garnett, R., vol. 31, https://proceedings.neurips.cc/paper/2018/file/a41b3bb3e6b050b6c9067c67f663b915-Paper.pdf, 2018.

Manzanas, R., Frías, M. D., Cofiño, A. S., and Gutiérrez, J. M.: Validation of 40 year multimodel seasonal precipitation forecasts: The role of ENS on the global skill, Journal of Geophysical Research, 119, 1708–1719, https://doi.org/10.1002/2013JD020680, 2014.

535 Maraun, D. and Widmann, M.: Statistical downscaling and bias correction for climate research, Cambridge University Press, 2018.

Maraun, D., Widmann, M., Gutiérrez, J. M., Kotlarski, S., Chandler, R. E., Hertig, E., Wibig, J., Huth, R., and Wilcke, R. A. I.: Earth's Future VALUE : A framework to validate downscaling approaches for climate change studies Earth's Future, pp. 1–14, https://doi.org/10.1002/2014EF000259, 2014.

Mühr, B., Kubisch, S., Marx, A., and Wisotzky, C.: CEDIM Forensic Disaster Analysis "Dürre & Hitzewelle Sommer 540 2018 (Deutschland)", 2018, 0–19, https://www.researchgate.net/publication/327156086_CEDIM_Forensic_Disaster_Analysis_Durre_Hitzewelle_Sommer_2018_Deutschland_Report_No_1, 2018.

Nagarajan, P., Warnell, G., and Stone, P.: Deterministic Implementations for Reproducibility in Deep Reinforcement Learning, CoRR, http://arxiv.org/abs/1809.05676, 2018.

NVIDIA: Framework Determinism, GitHub, https://github.com/NVIDIA/framework-determinism, last access: 12 December 2021, 2021.

545 Pang, B., Yue, J., Zhao, G., and Xu, Z.: Statistical Downscaling of Temperature with the Random Forest Model, Advances in Meteorology, 2017, https://doi.org/10.1155/2017/7265178, 2017.

Pastén-Zapata, E., Jones, J. M., Moggridge, H., and Widmann, M.: Evaluation of the performance of Euro-CORDEX Regional Climate Models for assessing hydrological climate change impacts in Great Britain: A comparison of different spatial resolutions and quantile mapping bias correction methods, Journal of Hydrology, 584, 124 653, https://doi.org/10.1016/j.jhydrol.2020.124653, 2020.

550 Plesser, H. E.: Reproducibility vs. Replicability: A brief history of a confused terminology, Frontiers in Neuroinformatics, 11, 1–4, https://doi.org/10.3389/fninf.2017.00076, 2018.

Pour, S. H., Shahid, S., and Chung, E. S.: A Hybrid Model for Statistical Downscaling of Daily Rainfall, Procedia Engineering, 154, 1424–1430, https://doi.org/10.1016/j.proeng.2016.07.514, 2016.

Quesada-Chacón, D., Barfus, K., and Bernhofer, C.: Climate change projections and extremes for Costa Rica using tailored predictors from 555 CORDEX model output through statistical downscaling with artificial neural networks, International Journal of Climatology, 41, 211–232, https://doi.org/10.1002/joc.6616, 2020.

Quesada-Chacón, D.: Singularity container for "Repeatable high-resolution statistical downscaling through deep learning", Zenodo [code], https://doi.org/10.5281/zenodo.5809705, last access: 11 July 2022, 2021a.

Quesada-Chacón, D.: Predictors and predictand for "Repeatable high-resolution statistical downscaling through deep learning", Zenodo [data 560 set], https://doi.org/10.5281/zenodo.5809553, last access: 11 July 2022, 2021b.

Quesada-Chacón, D.: dquesadacr/Rep_SDDL: Submission to GMD, Zenodo [code], https://doi.org/10.5281/zenodo.5856118, last access: 11 July 2022, 2022a.

Quesada-Chacón, D.: Rendered description of the source code of "Repeatable high-resolution statistical downscaling through deep learning", GitHub, https://github.com/dquesadacr/Rep_SDDL, last access: 11 July 2022, 2022b.

565   ReKIS: Regionales Klimainformationssystem Sachsen, Sachsen-Anhalt, Thüringen, https://rekis.hydro.tu-dresden.de, last access: 11 July 2022, 2021.

Riach, D.: TensorFlow Determinism (slides), https://bit.ly/dl-determinism-slides-v3, last access: 11 July 2022, 2021.

Richter, D.: Ergebnisse methodischer Untersuchungen zur Korrektur des systematischen Messfehlers des Hellmann-Niederschlagsmessers, Berichte des Deutschen Wetterdienstes 194, Offenbach am Main, 1995.

570   Ronneberger, O., Fischer, P., and Brox, T.: U-Net: Convolutional Networks for Biomedical Image Segmentation, CoRR, abs/1505.04597, http://arxiv.org/abs/1505.04597, 2015.

Rougier, N. P., Hinsen, K., Alexandre, F., Arildsen, T., Barba, L. A., Benureau, F. C., Brown, C. T., DeBuy, P., Caglayan, O., Davison, A. P., Delsuc, M. A., Detorakis, G., Diem, A. K., Drix, D., Enel, P., Girard, B., Guest, O., Hall, M. G., Henriques, R. N., Hinaut, X., Jaron, K. S., Khamassi, M., Klein, A., Manninen, T., Marchesi, P., McGlinn, D., Metzner, C., Petchey, O., Plesser, H. E., Poisot, T., Ram, K.,
575   Ram, Y., Roesch, E., Rossant, C., Rostami, V., Shifman, A., Stachelek, J., Stimberg, M., Stollmeier, F., Vaggi, F., Viejo, G., Vitay, J., Vostinar, A. E., Yurchak, R., and Zito, T.: Sustainable computational science: The ReScience Initiative, PeerJ Computer Science, 3, e142, https://doi.org/10.7717/peerj-cs.142, 2017.

Serifi, A., Günther, T., and Ban, N.: Spatio-Temporal Downscaling of Climate Data Using Convolutional and Error-Predicting Neural Networks, Frontiers in Climate, 3, 1–15, https://doi.org/10.3389/fclim.2021.656479, 2021.

580   Srivastava, R. K., Greff, K., and Schmidhuber, J.: Highway Networks, CoRR, http://arxiv.org/abs/1505.00387, 2015.

Stoddart, C.: Is there a reproducibility crisis in science?, Nature, pp. 3–5, https://doi.org/10.1038/d41586-019-00067-3, 2016.

Taylor, K., Stouffer, R., and Meehl, G.: An Overview of CMIP5 and the Experiment Design, Bulletin of the American Meteorological Society, 93, 485–498, https://doi.org/10.1175/BAMS-D-11-00094.1, 2012.

TOP500: AlphaCentauri - NEC HPC 22S8Ri-4, EPYC 7352 24C 2.3GHz, NVIDIA A100 SXM4 40 GB, Infiniband HDR200, https://top500.
585   org/system/179942/, last access: 11 July 2022, 2022.

Tripathi, S., Srinivas, V. V., and Nanjundiah, R. S.: Downscaling of precipitation for climate change scenarios: A support vector machine approach, Journal of Hydrology, 330, 621–640, https://doi.org/10.1016/j.jhydrol.2006.04.030, 2006.

Vandal, T., Kodra, E., Ganguly, S., Michaelis, A., Nemani, R., and Ganguly, A. R.: Generating high resolution climate change projections through single image super-resolution: An abridged version, International Joint Conference on Artificial Intelligence, pp. 5389–5393,
590   https://doi.org/10.24963/ijcai.2018/759, 2018.

von Storch, H., Zorita, E., and Cubasch, U.: Downscaling of Global Climate Change Estimates to Regional Scales: An Application to Iberian Rainfall in Wintertime, Journal of Climate, 6, 1161–1171, https://doi.org/10.1175/1520-0442(1993)006<1161:DOGCCE>2.0.CO;2, 1993.

Voosen, P.: Global temperatures in 2020 tied record highs, Science, 371, 334–335, https://doi.org/10.1126/science.371.6527.334, 2021.

Wackernagel, H.: Multivariate geostatistics: an introduction with applications, Springer, Berlin, 2010.

595   Wahl, S., Bollmeyer, C., Crewell, S., Figura, C., Friederichs, P., Hense, A., Keller, J. D., and Ohlwein, C.: A novel convective-scale regional reanalysis COSMO-REA2: Improving the representation of precipitation, Meteorologische Zeitschrift, 26, 345–361, https://doi.org/10.1127/metz/2017/0824, 2017.

Wilby, R. and Wigley, T.: Downscaling general circulation model output: a review of methods and limitations, Progress in Physical Geography: Earth and Environment, 21, 530–548, https://doi.org/10.1177/030913339702100403, 1997.

600   WMO: 2021 one of the seven warmest years on record, WMO consolidated data shows, https://public.wmo.int/en/media/press-release/2021-one-of-seven-warmest-years-record-wmo-consolidated-data-shows, last access: 11 July 2022, 2022.

Xu, B., Wang, N., Chen, T., and Li, M.: Empirical Evaluation of Rectified Activations in Convolutional Network, CoRR, http://arxiv.org/abs/1505.00853, 2015.

Zhou, Z., Rahman Siddiquee, M. M., Tajbakhsh, N., and Liang, J.: Unet++: A nested u-net architecture for medical image segmentation, Lecture Notes in Computer Science (including subseries Lecture Notes in Artificial Intelligence and Lecture Notes in Bioinformatics), 11045 LNCS, 3–11, https://doi.org/10.1007/978-3-030-00889-5_1, 2018.

605